SCIENCE BULLETIN
CHIAO-TUNG UNIV.
Vol.3,No.2(1969)

Silicon p-i-n Photodetector Using Internal Reflection Method

by

H. S. Lee* and S. M. Sze**

Abstract-A semiconductor photodetector is proposed which makes use of an internal reflection method to enhance the photoresponse. This method is to let the incident light be multiple - reflected in the detector so that a long distance is traveled and most of the photon energy is absorbed by the detector. The photodetector is particularly useful in detection of light with wavelengths near the intrinsic absorption edge.

Theoretical analysis of photoresponse for a p-i-n photodector is presented. Both the steady-state and time-dependent responses are derived; and the two important limiting cases with zero and infinite surface recombination velocities are taken as examples to illustrate the photoresponse.

The photodetectors are fabricaged from 4,000 Ω-cm, n-type, <111> oriented silicon wafers. Both sides of the wafer are polished with one side inclined half degree with respect to the other. The p^+n junction and the ohmic contact are formed by alloy method. The measured photoresponses for wavelengths of 1.0 um and 1.1 um (with absorption coefficients of 100 cm^{-1} and 3 cm^{-1} respectively) are in reasonalbe agreement with the theoretical predictions.

I. Introduction

One of the important optoelectronic devices [1] is the photovoltaic diode which has been developed for detection of coherent and incoherent radiations. When light is illuminated on a photovoltaic diode the total current is given by the sum of the reverse saturation current, I_S, and photocurrent I_{ph}. For ease of detection of the radiation it is required that I_{ph} should be large in comparison to I_S. For a given photodetector when the wavelength of the incident light approaches the intrinsic absorption edge of the dectector, e.g. using a Si photodiode to detect the 1.15 μm line of

* Formerly a graduate student of National Chiao-Tung Univ., Hsinchu, Taiwan, Republic of China
** Now with Bell Labs, Murray Hill, New Jersey, U.S.A.

a He-Ne laser, I_{ph} will drastically decrease. On the other hand, if one chooses another detector with smaller energy band gap, e.g. a germanium photodiode for the detection of the same wavelength, I_s will drastically increase. This is because that I_s is proportional to n_i, the intrinsic carrier concentration; and a semiconductor with smaller band gap generally has larger n_i.

In order to enhance the photocurrent for wavelengths near the intrinsic absorption edge, a photodetector using internal reflection method is herein proposed. This detector can give a reasonable large I_{ph} and at the same time keep I_s small.

Most of the photovoltaic diodes are operated under normal incidence, i.e. the incident light is perpendicular to the surface of the diode. For the proposed photodetector as shown in Fig. 1. the light is incident at an angle so chosen that the internal angle θ_1, is greater than the critical angle θ_c which is about 17° for Si.

In order to insure the multiple total reflection in the detector, the two planes of the diode should not be parallel as the usual diodes do, but rather be inclined at a small angle δ with each other. Thus the energy of the incident light will be confined within the detector, and an increase of photoresponse is expected.

To increase the quantum yield under multiple-reflection condition, both the diffusion length of minority carriers and the depletion width under reverse bias should be large. A wafer with low background doping and low dislocation density is needed. This is because that a defect-free low-doping samples can give both diffusion long length and wide depletion width at a given bias. In the present study a p-i-n diode is used, and the i region is approximated by a 4,000 Ω-cm, n type material.

We shall present in the next section the detailed device design theory which includes the steady-state and time-dependent photoresponses under various boundary conditions. The experimental results are given in Section III; and a discussion is presented in Section IV.

2. Device Design Theory

When a monochromatic light with wavelength λ is incident on a p-i-n diode and the absorption coefficient at this wavelength is (cm^{-1}), the generation rate of electron-hole pairs at a distance x from the surface is given by

$$g(x,t) = \eta\alpha\Phi\, e^{-\alpha x}(1 + me^{i\omega t}) \quad (1)$$

where η is the quantum efficiency which is defined as the number of electron-hole pairs produced by a photon, Φ the photon flux den-

sity at the surface in photons/cm^2-sec, m the degree of modulation which is smaller than unity, and ω the modulation angular frequency. We shall assume in the following derivations that the transit time of the generated carriers through the photodetector is small in comparison to the reciprocal of the angular frequency.

The total photocurrent density in a reverse biased diode consists of two components [2]:

$$J_{tot} = J_{dr} + J_d \tag{2}$$

where J_{dr} is the drift current density due to carriers generated inside the depletion region, and J_d is the diffusion current density due to carriers generated in the neutral region and diffused toward the depletion region. We shall consider the drift current component first.

Figure 2 (a) shows the variation of light intensity along the photodetector. Under the assumption of zero recombination within the depletion region [3], the drift current density is given by

$$\begin{aligned} J_{dr} &= q \int_0^W g(x,t)\,dx \\ &= q\eta\Phi(1+me^{i\omega t})(1-e^{-\alpha W}). \end{aligned} \tag{3}$$

We next consider the diffusion current component. The one-dimensional continuity equation for minority carriers (holes in the present case) in the neutral region can be expressed as

$$\frac{\partial p}{\partial t} = D_p \frac{\partial^2 p}{\partial x^2} + \frac{p_{no} - p}{\tau_p} + \eta\alpha\Phi e^{-\alpha x}(1+me^{i\omega t}) \tag{4}$$

where the symbols have their usual meanings. The solution [4] of the above equation is*

$$p(x,t) = [A_1 e^{\frac{x}{L_p}} + A_2 e^{-\frac{x}{L_p}} + p_{no} + \frac{\alpha L_p^2 \Phi n e^{-\alpha x}}{D_p(1-\alpha^2 L_p^2)}]$$

$$+me^{i\omega t}\left(B_1 e^{\frac{x}{L_p^*}} + B_2 e^{-\frac{x}{L_p^*}} + \frac{\alpha L_p^{*2}\Phi n e^{-\alpha x}}{D_p(1-\alpha^2 L_p^{*2})}\right) \tag{5}$$

where $L_p \equiv (D_p\tau_p)^{1/2}$ is the diffusion length of minority carriers, $L_p^* \equiv L_p/(1+i\omega\tau_p)^{1/2}$, and A_1, A_2, B_1, B_2 are constants to be determined from the boundary conditions.

Case 1. As shown in Fig. 2(b) with n+side incident i.e. the light intensity decay exponentially from n^+ to p^+ layer. The boundary conditions at steady state ($t > 3\tau_p$) and for applied reverse voltage $V >> \frac{KT}{q}$, are given as

$$S\left[p(0,t)-p_{no}\right] = D_p \frac{\partial p(x,t)}{\partial x}\Big|_{x=0}$$

$$p(x_1,t) \simeq 0 \tag{6}$$

where S is surface recombination velocity.

The constants in Eq. 5 can be evaluated using Eq. 6. Substitution of the results into the current density equation

$$J = -qD_p \frac{\partial p(x,t)}{\partial x}\Big|_{x=x_1} \tag{7}$$

yields the diffusion current component:

$$J_{d1} = J_{o1} + q\eta\Phi_1\left[F(L_p, x_1) + me^{i\omega t}F(L_p^*, x_1)\right] \tag{8}$$

where

$$J_{o1} \equiv \frac{qD_p p_{no}\left(S\cosh\frac{x_1}{L_p} + \frac{D_p}{L_p}\sinh\frac{x_1}{L_p}\right)}{L_p\left(S\sinh\frac{x_1}{L_p} + \frac{D_p}{L_p}\cosh\frac{x_1}{L_p}\right)}$$

$$F(L_p, x_1) \equiv \frac{\alpha L_p\left\{S+\alpha D_p - e^{-\alpha x_1}\left[(S+\alpha D_p)\cosh\frac{x_1}{L_p} + \left(\frac{D_p}{L_p} + S\alpha L_p \sinh\frac{x_1}{L_p}\right)\right]\right\}}{(\alpha^2 L_p^2 - 1)\left(S\sinh\frac{x_1}{L_p} + \frac{D_p}{L_p}\cosh\frac{x_1}{L_p}\right)}$$

and $F(L_p^*, x_i)$ is identical to $F(L_p, x_i)$ except that L_p^* replaces L_p.

Figure 3 shows a typical set of $F(L_p, x_i)$ for a photodetector with minimum beight $H = 744\,\mu m$, $L_p = 139\,\mu m$, and $\delta = 0.5°$ (see Fig. 1). The two limiting cases of $S=0$ (corresponding to perfect reflecting contact) and $S=\infty$ (corresponding to perfect ohmic contact) are considered. The abssica is the reflection time which represents the variation x_i as the light is multiple - reflected. It is well known that after each reflection the angle is increased by 2 , e.g. $\theta_2 = \theta_1 + \delta 2$ as shown in Fig. 4 where $x_i \equiv (d_i - w_i)$. Hence as the reflection time increases, x_i increases. In the plot the absorption coefficient α is considered as a parameter.

Case 2. p^+ side incident as shown in Fig. 2(c) i.e. the light intensity decays exponentially from p^+ to n^+ layer.

The boundary conditions are now

$$p(w_j, t) \cong 0$$

$$S[p(w_j + x_j, t) - p_{no}] = D_p \frac{\partial p(x,t)}{\partial x} | x = w_j + x_j . \tag{10}$$

From the above conditions and the relation

$$J = -qD_p \frac{\partial p(x,t)}{\partial x} | x = w_j$$

we obtain the diffusion current component:

$$J_{d2} = -J_{o2} - q\eta\Phi_j e^{-\alpha w_j} [G(L_p, x_j) + me^{i\omega t} G(L_p^*, x_j)] \tag{11}$$

where

$$J_{o2} \equiv \frac{qD_p p_{no}(S\cosh\frac{x_j}{L_p} - \frac{D_p}{L_p}\sinh\frac{x_j}{L_p})}{L_p(S\sinh\frac{x_j}{L_p} - \frac{D_p}{L_p}\cosh\frac{x_j}{L_p})}$$

$$G(L_p, x_j) \equiv \frac{\alpha L_p[(S+\alpha D_p)\cosh\frac{x_j}{L_p} - (\frac{D_p}{L_p} + S\alpha L_p)\sinh\frac{x_j}{L_p} - (S+\alpha D_p)e^{-\alpha x_j}]}{(\alpha^2 L_p^2 - 1)(\frac{D_p}{L_p}\cosh\frac{x_j}{L_p} - S\sinh\frac{x_j}{L_p})}$$

Table I, where the diode number is arbitrary named, with larger number corresponding to larger area and more reflection times.

The experimental setup for the photoresponse measurement is shown in Fig. 7. The light is incident form the p side in order to obtain larger response. The filter system is a combination of infrared and silicon filters. The photocurrent is measured with the help of an oscilloscope. A linear amplifier is inserted at the input stage of the oscilloscope to increase the gain.

For incident light with wavelength 1.0 μm and power density 7.125×10^{-4} watts/cm^2, the quantum efficiency is 11.9% with an absorption coefficient of 100 cm^{-1}. The theorectical and experimental results are shown in Fig. 8 where the solid line represents the case of infinite surface recombination velocity ($S = \infty$) and the dashed line for $S = 0$. Because of the large value of α the diffe - rence are, however, quite small. The agreement between the experimental data and the theoretical curves are reasonably good.

Also shown in Fig. 8 are results for the case of an incident light with wavelength 1.1 μm and power density 1.585×10^{-4} watts/ cm^2. The corresponding absorption coefficient is 3 cm^{-1}, and the quantum efficiency is only 0.595%. Apparently, the experimental results are in closer agreement with the case of infinite surface recombination velocity.

4. Discussion

When light is incident from p+ side and for the case of large absorption coefficient, α most of photoenergy is absorbed in the depletion region in the first trip that light has traveled. The amount of light energy that has been left after the light pass through the depletion region of the first trip is only $e^{-\alpha w}$ of the total incident energy, where w is the width of depletion region. Since α is large, the value of $e^{-\alpha w}$ approaches zero; so that the property of neutral region has little effect on the tatal photocurrent. Thus the n+ layer which may serve either as perfect reflector ($S = 0$) or perfect ohmic contact ($S = \infty$) is immaterial to the measured current. This is the reason that the two theorical curves for α = 100 cm^{-1} in Fig. 8 are virtually identical.

However, when the product of absorption coefficient and the width of depletion region is much less than unity, the diffusion current density J_d is the predominant term in Eq. 2 . The property of the n layer is now an important factor to the photocurrent. In the case of $\alpha = 3$ cm^{-1} $J_{tot}(S = 0) \cong 2 J_{tot}(S = \infty)$.

It is shown in Fig. 8 that for the case of $\alpha = 3$ cm^{-1}, the n layer serves as a ohmic contact layer rather than a reflecting layer.

It is conceivable that when an antireflection coating[5] is deposited on the incident surface, more light will be absorbed by the detector and an increase of the photoresponse is expected.

Since the planar technology can control the diffusion depth precisely, it is recommended to use low temperature diffusion (at temperatures less than 1000°C) to form the n and p layers. At higher temperatures, however, more dislocations and defects may be introduced to the diode.

The breakdown voltage of these diodes are greater than 200 volts and the applied voltage in the experimental study is only 10 volts. Hence the avalanche multiplication effect can be neglected. If the applied voltage is close to the breakdown voltage, then the multiplication factor M(V) should be multiplied to Eq. 15 .

Acknowledgements

The authors wish to thank Dr. C. C. Wang of Sperry Rand Research Center for his constructive suggestions and comments and Mr. Loya of Bell Laboratories for providing the polished high resistivity silicon wafers.

Thanks are also due to the members of the semiconductor laboratory, particularly Miss S. R. Shyu, Mr. Y. J. Chang, and Mr. M. Y Kuo for their technical assistance; and to Miss C. Y. Han and Miss C. C. Yuan of the computer center for their help in programming and computation.

References

1. For a general reference on optoelectronic devices, see for example, S. M. Sze, "Physics of Semiconductor Devices", Chap. 12, p. 625-p. 686, John Wiley and Sons, New York, 1969.
2. W. W. Gartner, "Depletion-Layer Photoeffects in Semiconductors", Phys. Rev., Vol, 116, No. 1. pp. 84-87, Oct. 1, 1959.
3. W. Van Roosbroeck, "Current-Carrier Transport and Photoconductivity in Semiconductors with Trapping," Phys. Rev., Vol. 119, No. 2, pp. 636-652, July 15, 1960.
4. D. E. Sawyer and R. H. Rediker, "Narrow Base Germanium Photodiodes", Proc. IRE, Vol. 46, No. 6, pp. 1122 - 1130 June 1958.
5. M. V. Schneider, "Schottky Barrier Photodiodes with Antireflection Coating," Bell Syst. Tech. J., Vol. 45, No. 9, pp 1611 - 1638, Nov. 1966.

and $G(L_p^*, x_i)$ is identical to $G(L_p, x_i)$except that L_p is replaced by L_p^*.

The function $G(L_p, X_j)$ is also shown in Fig. 3 with device parameters identical to that for case 1.

The total current density for single pass of light from n^+ to p^+ layer can be obtained from Eqs. 2 , 3 and 8

$$J_{t1}(\Phi_i, x_i, w_i) = J_{o1} + q\eta\Phi_i\{[e^{-\alpha x_i}(1-e^{-\alpha w_i}) + F(L_p^*, x_i)] + me^{i\omega t}[e^{-\alpha x_i}(1-e^{-\alpha w_i}] + F(L_p^*, x_i)]\} \tag{13}$$

where Φ_i is the ith time light flux density at $x = 0$, x_i and w_i are the corresponding widths of neutral region and depletion region respectively.

The total current density for a single pass of light from p^+ to n^+ layer can be obtained similarly:

$$J_{t2}(\Phi_j, x_j, w_j) = -J_{o2} - qn\Phi_j\{[1-e^{-\alpha w_j} + G(L_p, x_j)\, e^{-\alpha w_j}] + me^{i\omega t}[1-e^{-\alpha w_j} + G(L_p^*, x_j)e^{-\alpha w_j}]\}. \tag{14}$$

Under internal multiple reflections as shown in Fig. 4, the current components along the x direction will be summed up. The total current density J_{tot} is finally obtained as

$$J_{tot} = \sum_{i=1}^{n} J_{t1}(\Phi_i, d_i' - w_i', w_i')\cos\theta_i - \sum_{j=1}^{n} J_{t2}(\Phi_j, d_j - w_j, w_j)\cos\theta_j$$

where $\Phi_i = \Phi_o \exp[-\alpha \sum_{\beta=0}^{i-1} (d_{\beta+1} + d'_\beta)]$

$$\Phi_j = \Phi_o \exp[-\alpha \sum_{\beta=0}^{i-1} (d_\beta + d'_\beta)]$$

and Φ_o is the initial light flux density incident on the detector, $d_o = d'_o = 0$, and the indices i and j run from 1 to n which is the number of reflections within the detector.

Figure 5 shows the calculated time-dependent component of total current density as a function of reflection times for S = 0 and S=∞, with $\omega\tau_p << 1$.

Figute 6 shows the calculated light traveling path within the diode and the length of active region L (as shown in Fig. 1) normalized by the factor H, as a function of reflection times. For example, when the absorption coefficient of the incident light is 3 cm^{-1}, the light traveling path should be about $1/\pi$ or 0.33 cm. If H=744 μm we have to let the incident light be reflected twice. Hence the length of the active region should be 1.04 cm (since L/H = 1.4) for a δ of 0.5^o

3. Experiments

The samples used in the experiment are n-type silicon wafers, 4,000 Ω-cm, one inch in diameter, and <111> oriented. The lifetime and diffusion length of minority carriers in the sample are determined to be 1.5×10^{-3} sec and 1390 μm respectively. Both sides of the wafer are polished to a mirror finish. One side is inclined a half degree with respect to the other.

After cleaning, the wafer is put into an evaporator and 3000A aluminimu film is deposited through a metal mask which contains windows of various sizes, After deposition the sample is heated under forming gas to a temperature slightly higher than the Al-Si eutectic temperature of 580^oC for 5 min, so that the alloy serves as the p^+ contact to the n-type high-resistivity material.

To form the n ohmic contact the alloy Au-Sb is deposited onto the other face of the wafer and is heated under forming gas to $380^o C$ for 5 min. From the capacitance measurement of these diodes, it is confirmed that they are one-sided abrupt junctions. The diffusion constant for these diodes is 12.9 cm^2/sec and the depletion width at 10V reverse bias is 96 μm.

The exact dimensions of the fabricated diodes are listed in

Table I. Dimensions of the photodetectors

No.	H(um)	Area(cm^2)	Reflection times in photodetector
1	784	6.94×10^{-3}	6
2	781	11.75×10^{-3}	8
3	744	22.18×10^{-3}	10
4	731	28.27×10^{-3}	11
5	670	44.32×10^{-3}	13

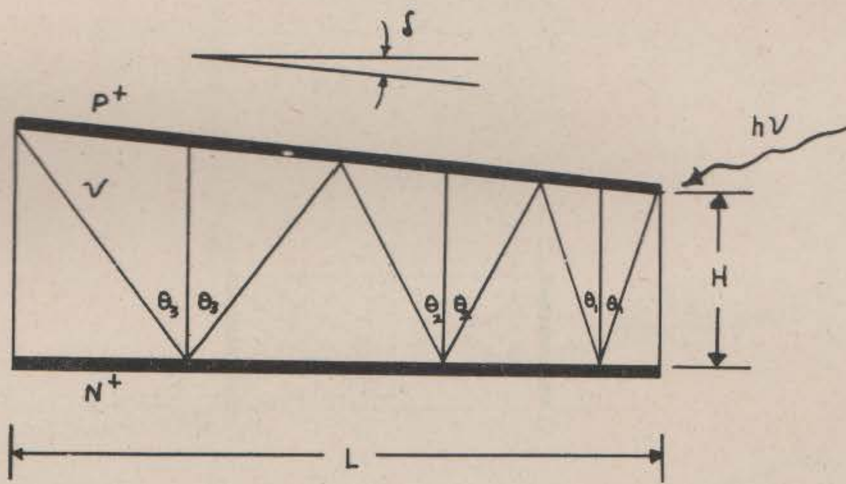

Fig. 1. A schematic diagram of a multiple-reflection photodetector.

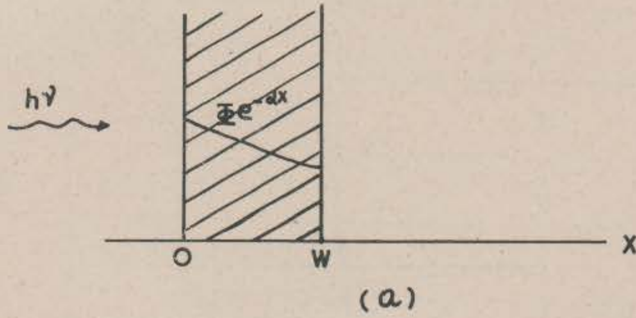

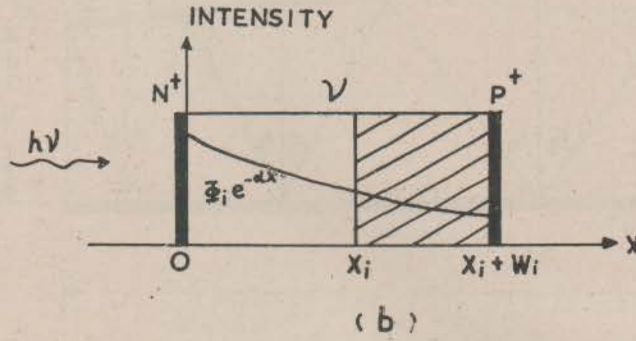

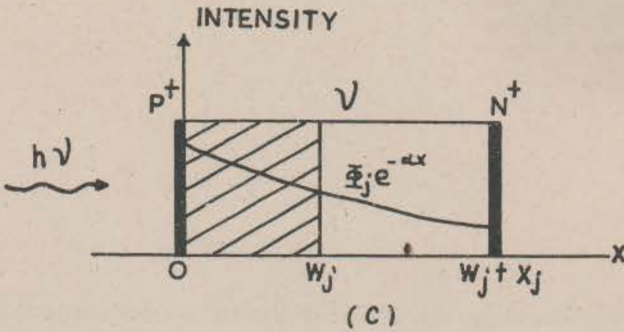

Fig. 2. (a) Light intensity distribution in the depletion region.

(b) Light intensity distribution in a p-i-n diode when the light is incident from n side.

(c) Light intensity distribution in a p-i-n diode when the light is incident from p side.

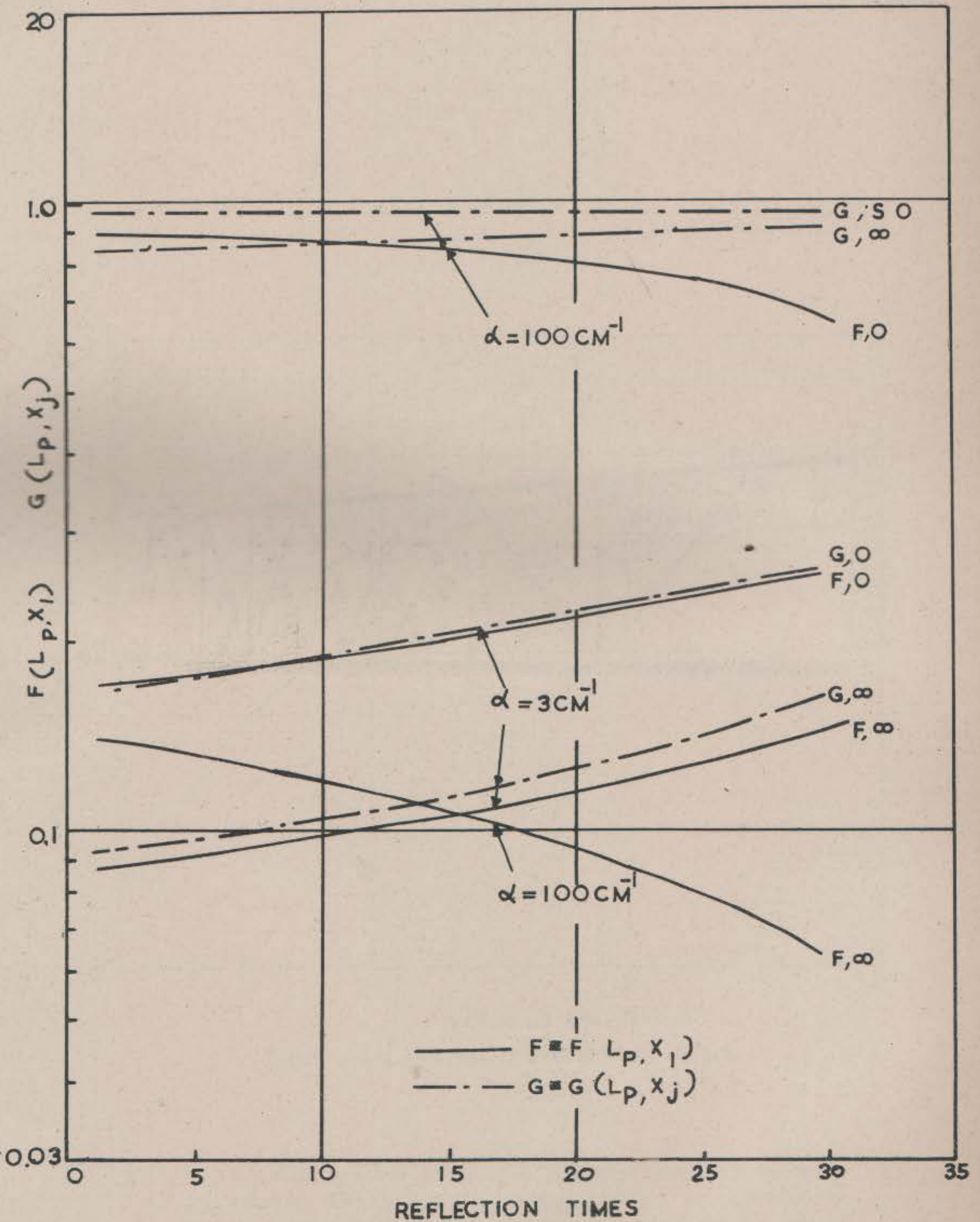

Fig. 3. Functions $F(L_p, x_i)$ and $G(L_p, x_i)$ versus reflection times with devices parameters $L_p = 139$ um, $H = 744$ um, $\delta = 0.5^o$ and $D_p = 12.9\ cm^2/sec$. The solid line is for the case of $S = \infty$, and dashed line for $S = 0$.

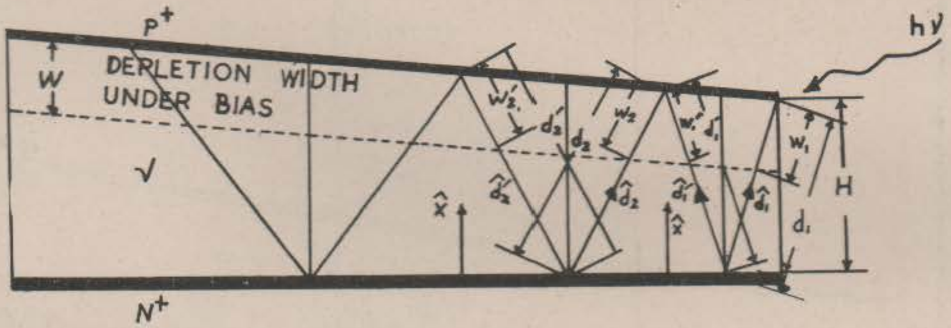

Fig. 4. Light traveling path in a p-i-n diode.

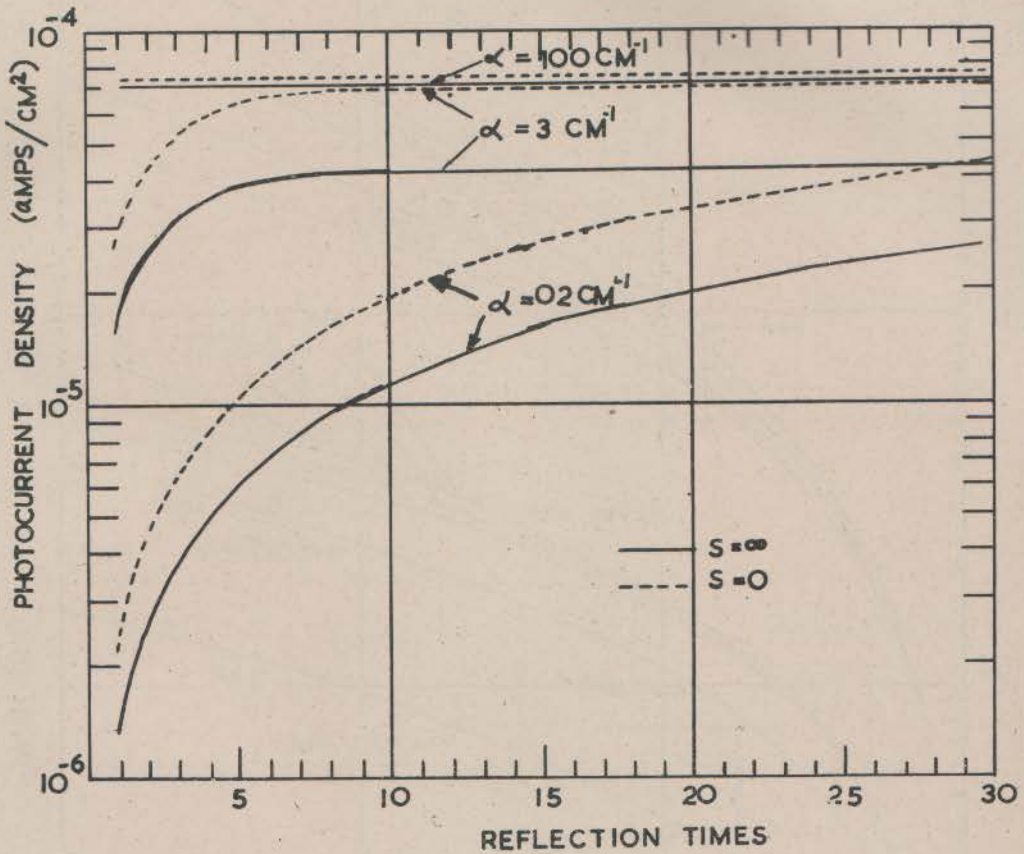

Fig. 5 . Current density versus reflection times for various absorption coefficients. The device parameters used in the calculation are the same as in Fig. 3. The solid line is for $S = \infty$, dashed line for $S = 0$.

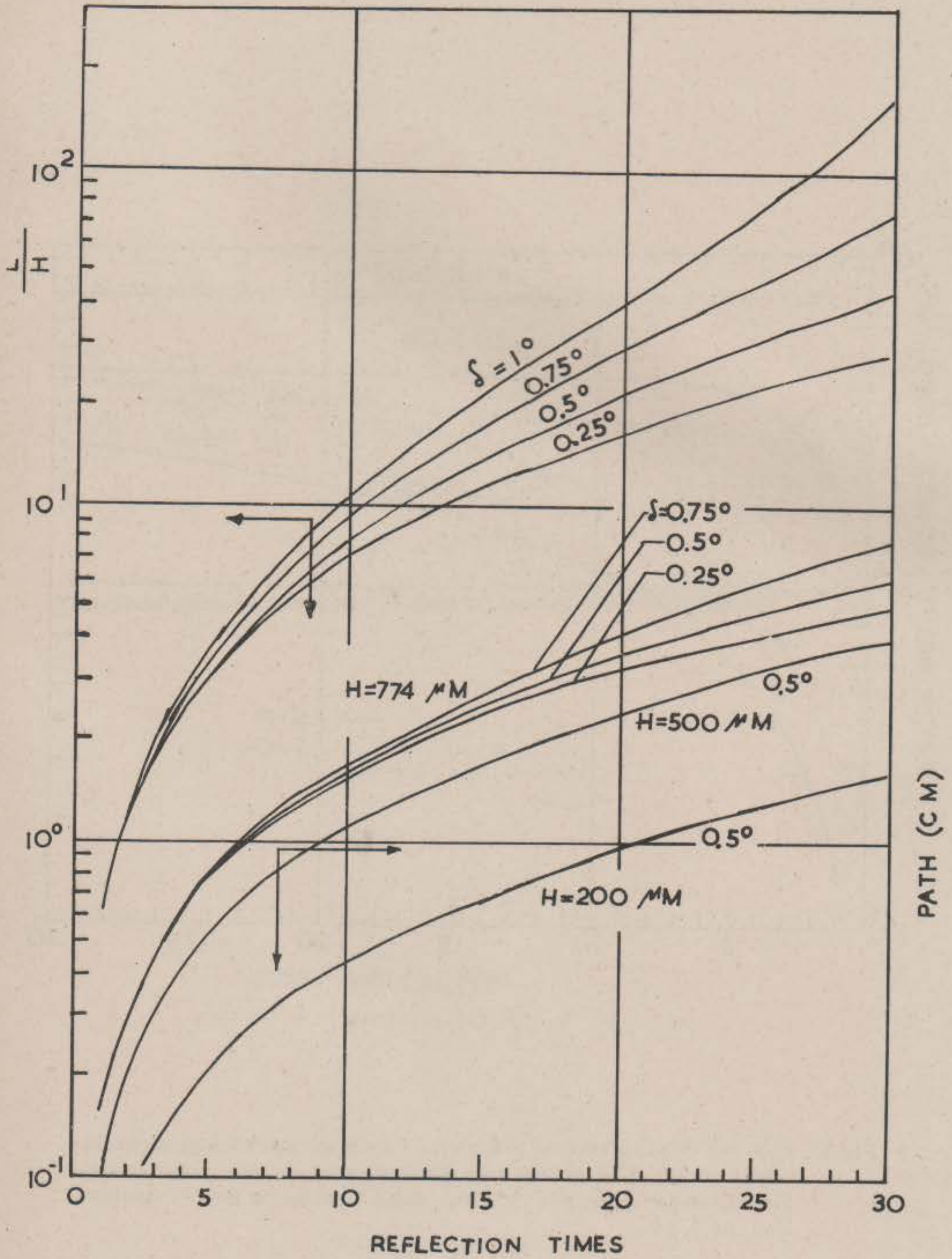

Fig. 6. Light traveling path and L/H versus reflection times.

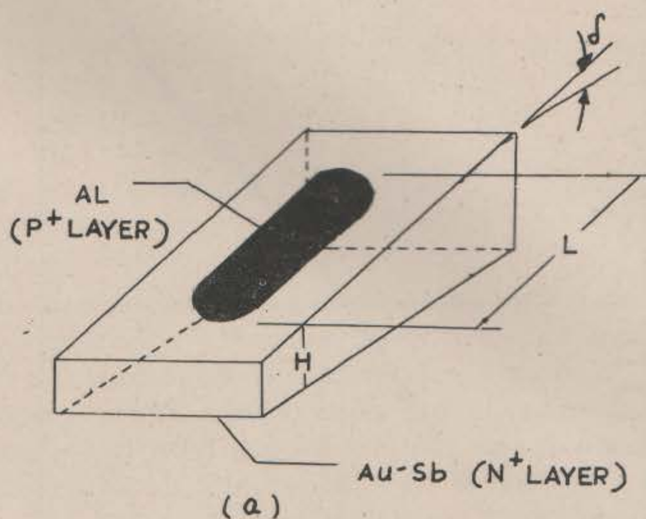

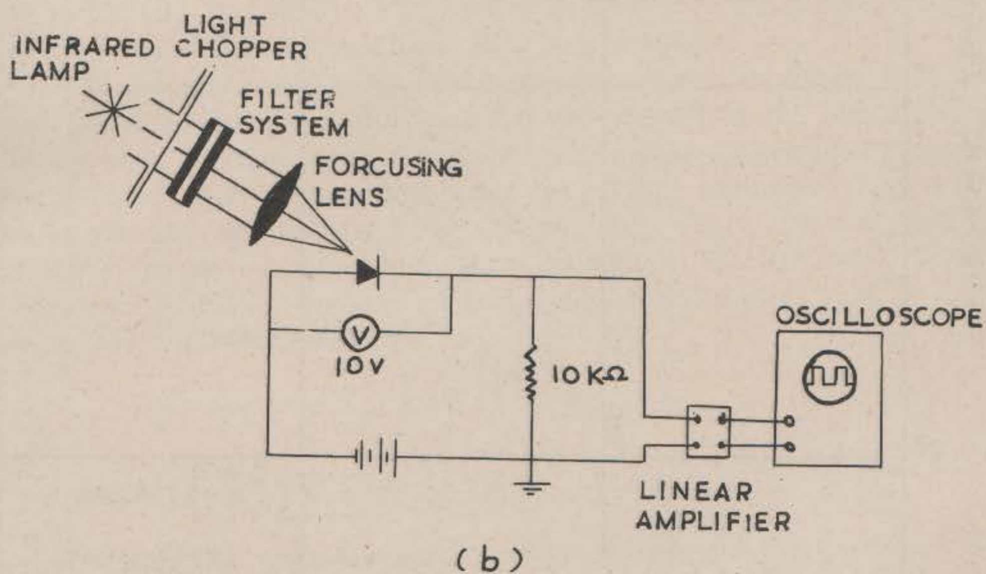

Fig. 7. (a) Fabricated diode structure.

(b) Measurement setup.

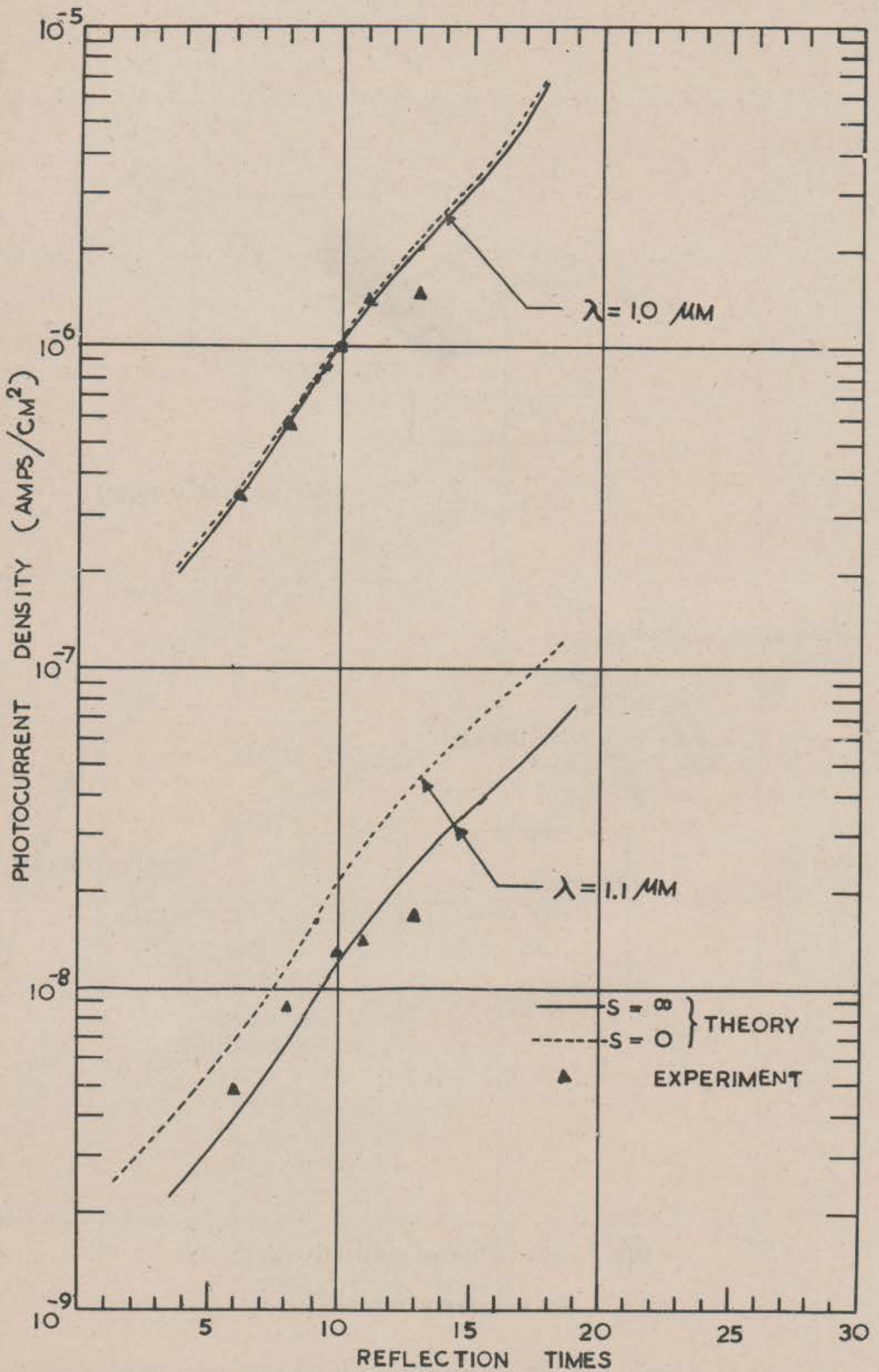

Fig. 8. Comparison of experimental results (data points) and theoretical calculations (solid lines for $S = \infty$, and doted lines for $S = 0$). The upper set is for the case of $\alpha = 1.0$ um. $\eta = 11.9\%$ and input power $W_{in} = 7.125 \times 10^{-4}$ watt/cm^2. The lower set is for $\alpha = 1.1$ um, $n = 0.595\%$, and $W_{in} = 1.585 \times 10^{-4}$ watts/cm^2.